New Capabilities and Improvements to the High-Order Glenn Flux Reconstruction Code

Seth Spiegel, Dennis Yoder, James DeBonis, H.T. Huynh
Gregory Heinlein, Michael Borghi, and Nicholas Georgiadis

NASA Glenn Research Center

2025 AIAA SciTech Forum
Orlando, FL
January 6, 2025

Outline

GFR Background

New Capabilities and Improvements

- Improved Time-Advancement Methods
- 3D Mixed Element Capability
- Rotating Turbomachinery Capability

Results

- Spacecraft Cabin Ventilation Fan

Summary

GFR Background

GFR – Glenn Flux Reconstruction code

Unstructured CFD code based on the high-order flux reconstruction (FR) method with particular focus on providing a large-eddy simulation (LES) capability for complex aeropropulsion flows.

Why the flux reconstruction (FR) method?

- **High-order (> 2nd order) methods are ideal for LES.**
- **Unstructured methods are best for complex geometries.**
- **Created by our coworker H.T. Huynh here at NASA Glenn.**
- **Combines several existing high-order finite-element type methods under a single framework.**
  - Different versions of discontinuous Galerkin (DG) methods; Spectral-Difference, Spectral-Volume, and has been expanded to generate new methods.
- **Arbitrary order of accuracy through a single input parameter.**
  - Specify solution polynomial degree P, giving P+1 order of accuracy.
- **Scales very well for very large numbers of parallel processes (10k+).**

New Capabilities and Improvements

Improved Time-Advancement Methods

Runge-Kutta Method	Status	Stages	Order	$\Delta t / \Delta t_{SSP3}$	Time-to-Solution Speedup vs SSP3
Strong-Stability-Preserving (SSP) 3/3	Baseline	3	3	1.0	1.0
SSP 5/4	Existing	5	4	1.889	1.22
Carpenter-Kennedy 5/4 Low Storage	Existing	5	4	1.556	0.99
[illegible]	[illegible]	5	3	[illegible]	1.08
[illegible]	[illegible]	[illegible]	[illegible]	[illegible]	1.33
[illegible]	[illegible]	[illegible]	[illegible]	1.889	1.02
VO 15/4	New	15	4	6.0	1.33
[illegible]	[illegible]	[illegible]	[illegible]	2.556	1.05
VO 16/5	New	16	5	5.833	1.18
[illegible]	[illegible]	[illegible]	[illegible]	[illegible]	[illegible]
Dormand-Prince EP 7/5(4)	New	6	5(4)	1.222	0.64
Dormand-Prince EP 12/8(7)	New	12	8(7)	2.378	0.61
Optimized EP 5/3(2) FSAL	New	5	3(2)	1.767	1.09
Optimized EP 5/3(2)	New	5	3(2)	1.767	1.10
Optimized EP 9/4(3) FSAL	New	9	4(3)	3.333	1.22
Optimized EP 9/4(3)	New	9	4(3)	3.556	1.25
Optimized EP 10/5(4) FSAL	New	10	5(4)	2.778	0.85

Baseline time-advancement method

- Strong Stability Preserving (SSP) 3-stage/3rd-order Explicit Runge-Kutta (ERK) method.
- This has been used for nearly all previous GFR simulations.

New Capabilities and Improvements

Improved Time-Advancement Methods

8 Existing ERK Methods

12 New Optimized ERK Methods

8 New Embedded Pair ERK Methods with Adaptive Time-Stepping

Runge-Kutta Method	Status	Stages	Order	$\Delta t/\Delta t_{SSP3}$	Time-to-Solution Speedup vs SSP3
Strong-Stability-Preserving (SSP) 3/3	Baseline	3	3	1.0	1.0
SSP 5/4	Existing	5	4	1.889	1.22
Carpenter-Kennedy 5/4 Low Storage	Existing	5	4	1.556	0.99
Vortex-Optimized (VO) 5/3	New	5	3	1.667	1.08
VO 11/3	New	11	3	4.444	1.33
VO 6/4	New	6	4	1.889	1.02
VO 15/4	New	15	4	6.0	1.33
VO 8/5	New	8	5	2.556	1.05
VO 16/5	New	16	5	5.833	1.18
Advection-Optimized (AO) 16/5	New	16	5	5.0	0.98
Dormand-Prince EP 7/5(4)	New	6	5(4)	1.222	0.64
Dormand-Prince EP 12/8(7)	New	12	8(7)	2.378	0.61
Optimized EP 5/3(2) FSAL	New	5	3(2)	1.767	1.09
Optimized EP 5/3(2)	New	5	3(2)	1.767	1.10
Optimized EP 9/4(3) FSAL	New	9	4(3)	3.333	1.22
Optimized EP 9/4(3)	New	9	4(3)	3.556	1.25
Optimized EP 10/5(4) FSAL	New	10	5(4)	2.778	0.85

New Capabilities and Improvements

Improved Time-Advancement Methods

	Runge-Kutta Method	Status	Stages	Order	$\Delta t/\Delta t_{SSP3}$	Time-to-Solution Speedup vs SSP3
	Strong-Stability-Preserving (SSP) 3/3	Baseline	3	3	1.0	1.0
	SSP 5/4	Existing	5	4	1.889	1.22
	Carpenter-Kennedy 5/4 Low Storage	Existing	5	4	1.556	0.99
	Vortex-Optimized (VO) 5/3	New	5	3	1.667	1.08
Classic CFL time-stepping	**VO 11/3**	**New**	**11**	**3**	**4.444**	**1.33**
	VO 6/4	New	6	4	1.889	1.02
	VO 15/4	**New**	**15**	**4**	**6.0**	**1.33**
	VO 8/5	New	8	5	2.556	1.05
	VO 16/5	New	16	5	5.833	1.18
	Advection-Optimized (AO) 16/5	New	16	5	5.0	0.98
	Dormand-Prince EP 7/5(4)	New	6	5(4)	1.222	0.64
	Dormand-Prince EP 12/8(7)	New	12	8(7)	2.378	0.61
	Optimized EP 5/3(2) FSAL	New	5	3(2)	1.767	1.09
Adaptive time-stepping	Optimized EP 5/3(2)	New	5	3(2)	1.767	1.10
	Optimized EP 9/4(3) FSAL	**New**	**9**	**4(3)**	**3.333**	**1.22**
	Optimized EP 9/4(3)	**New**	**9**	**4(3)**	**3.556**	**1.25**
	Optimized EP 10/5(4) FSAL	New	10	5(4)	2.778	0.85

New Capabilities and Improvements

Improved Time-Advancement Methods

Runge-Kutta Method	Status	Stages	Order	$\Delta t/\Delta t_{SSP3}$	Time-to-Solution Speedup vs SSP3
Strong-Stability-Preserving (SSP) 3/3	Baseline	3	3	1.0	1.0
SSP 5/4	Existing	5	4	1.889	1.22
Carpenter-Kennedy 5/4 Low Storage	Existing	5	4	1.556	0.99
Vortex-Optimized (VO) 5/3	New	5	3	1.667	1.08
VO 11/3	**New**	**11**	**3**	**4.444**	**1.33**
					1.02
VO 15/4	New	15	4	6.0	**1.33**
					1.05
					1.18
					0.98
					0.64
					0.61
					1.09
					1.10
Optimized EP 9/4(3) FSAL	**New**	**9**	**4(3)**	**3.333**	**1.22**
Optimized EP 9/4(3)	**New**	**9**	**4(3)**	**3.556**	**1.25**
Optimized EP 10/5(4) FSAL	New	10	5(4)	2.778	0.85

Classic CFL time-stepping

Adaptive time-stepping

Significance:

- Large scale-resolving simulations can take weeks to produce quality time-averaged solutions.
- A time-to-solution speedup of 20-30% can eliminate **days** of expensive run time.

New Capabilities and Improvements

3D Mixed Element Capability

Added support for grid topologies containing tetrahedra, pyramid, and/or prism elements.

Required significant updates to many parts of the code:

- Preprocessing, including periodic boundary conditions.
- Creating geometry-generic algorithms to create the matrix operators needed for the FR method.
  - Interpolation, derivative, correction, projection, filtering, switching between nodal/modal forms
- Generating high-order face connectivities needed for cell interface operations.
- Post-processing algorithms for exporting high-order mixed-element solution data using parallel CGNS.

Taylor-Green Vortex Problem

Instantaneous contours of vorticity magnitude at t*=8

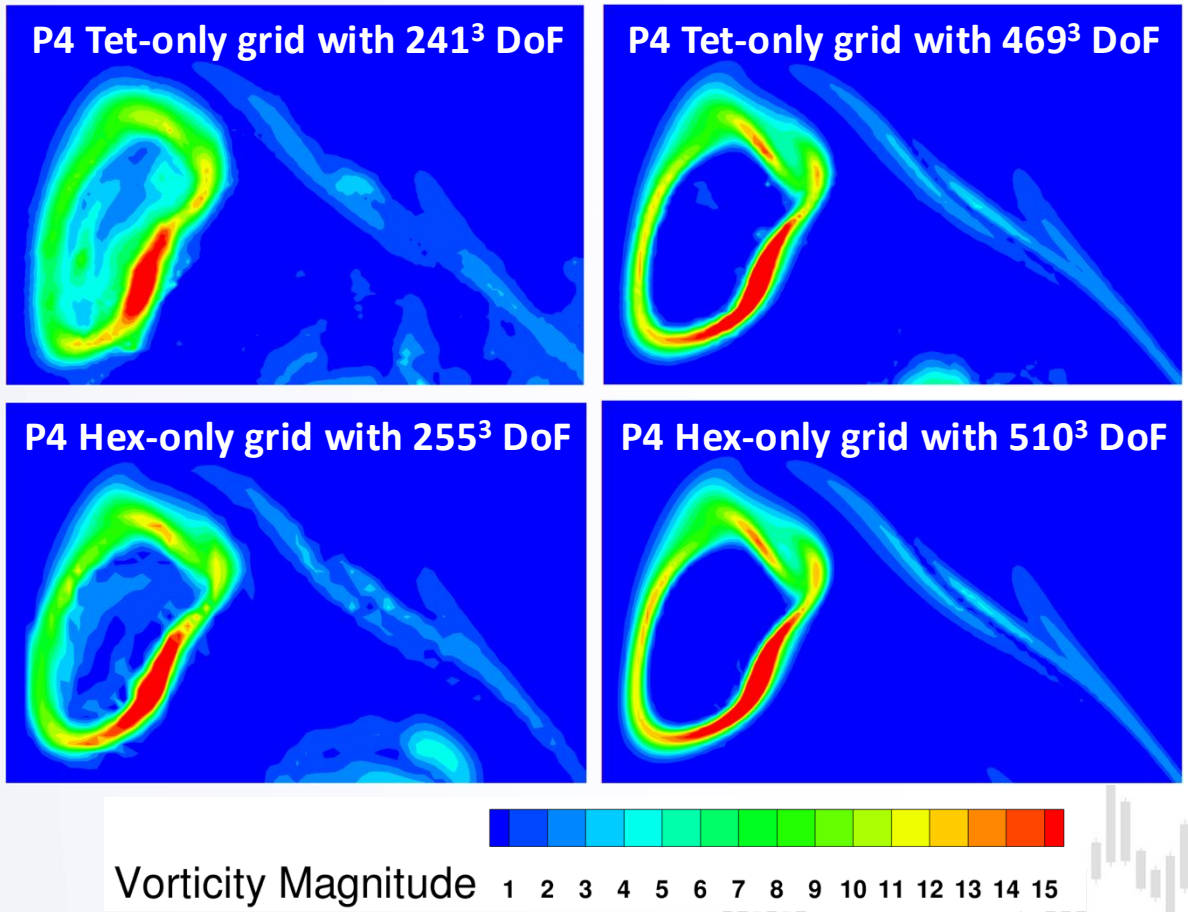

New Capabilities and Improvements

Rotating Turbomachinery Capability

Successfully added rotating reference frame capability to GFR.

- This capability allows the user to specify arbitrary grid rotation about all three Cartesian axes.
- Traditional turbomachinery codes tend to only allow rotation about a single primary axis.

Added rotated periodic boundary conditions.

- This can significantly reduce computational costs of turbomachinery flows that contain rotational symmetries.

Results

Spacecraft Cabin Ventilation Fan

Geometry

- Single-stage fan with 9 rotor blades and 11 stators
- Approximately 9 in. long with 4 in. diameter
- Design conditions
  - 12,000 RPM
  - 150.3 ft^3/min (CFM) volumetric flow rate
  - 3.64 in. of water stagnation pressure rise
  - @ 70°F and 14.7 psia

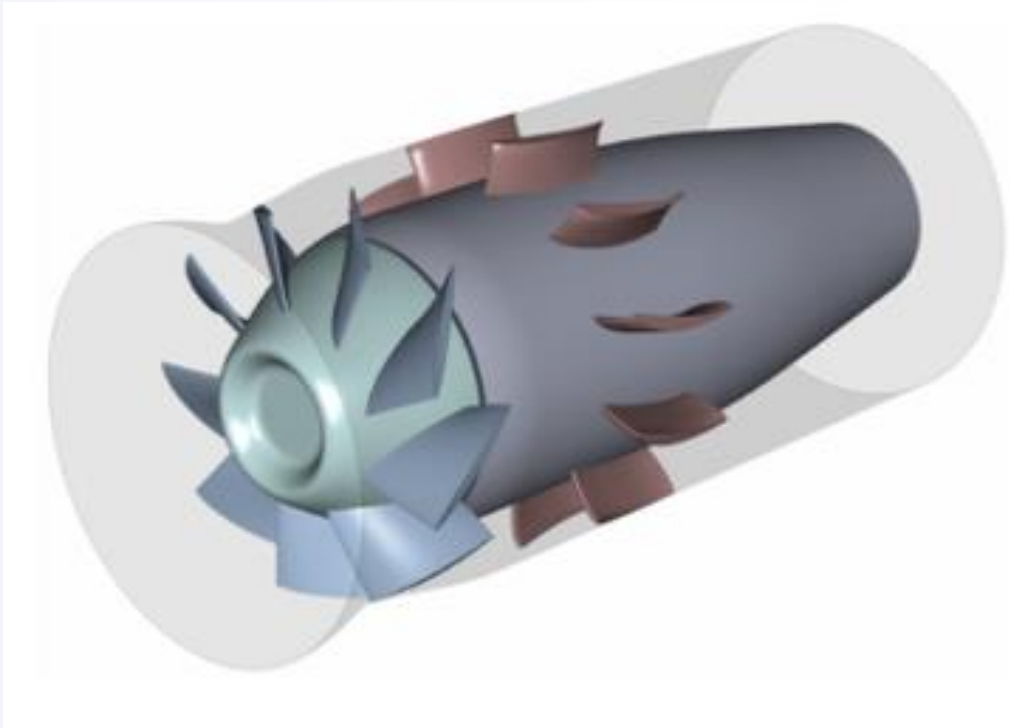

Fan Geometry

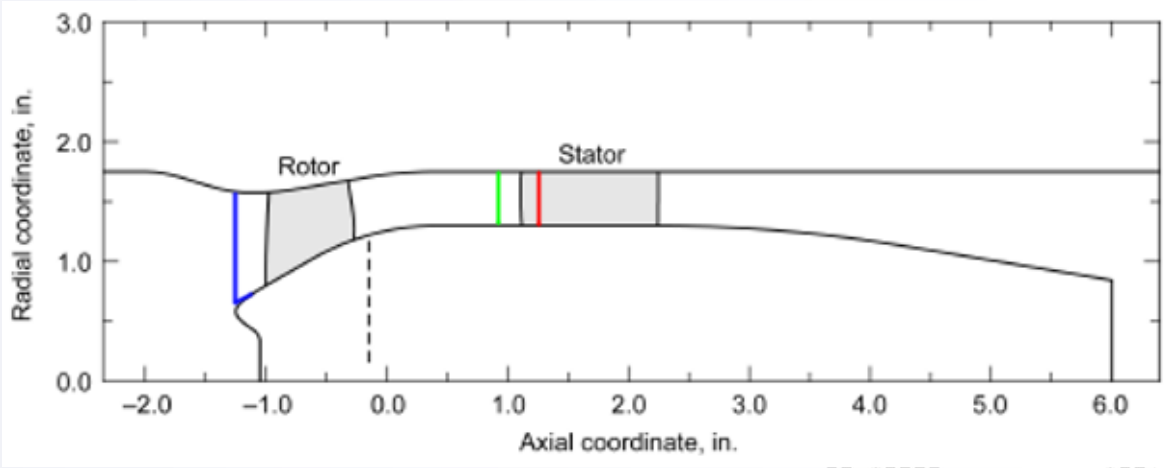

Meridional View

Results

Spacecraft Cabin Ventilation Fan

Computational Domain

- Single blade with rotationally periodic domain of 40°.
- Sponge layer was added at outflow to help damp out non-physical pressure waves reflecting off the outflow boundary.
  - The sponge region did not include the stator blade.
- The hub geometry was modified at the inflow to a shallower incident angle.
- The air gap between the rotating and stationary parts of the hub was removed, and the stationary part of the hub was changed to rotating.

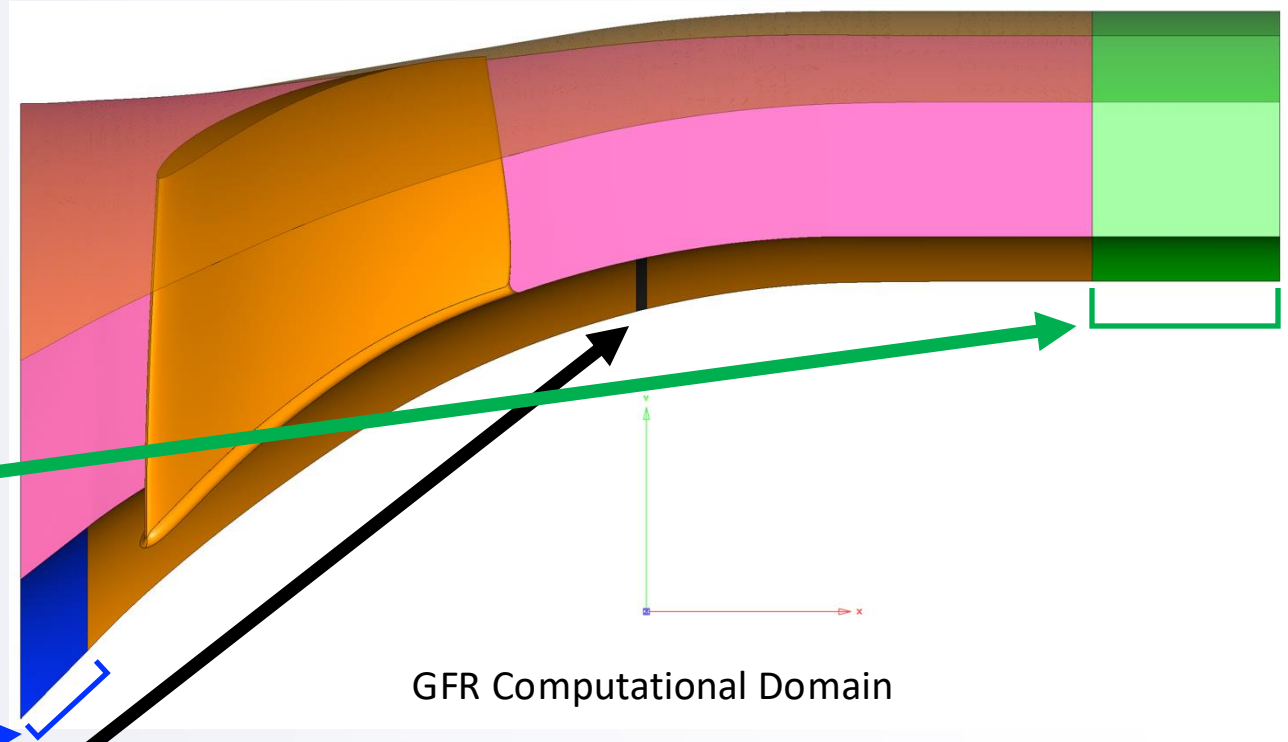

GFR Computational Domain

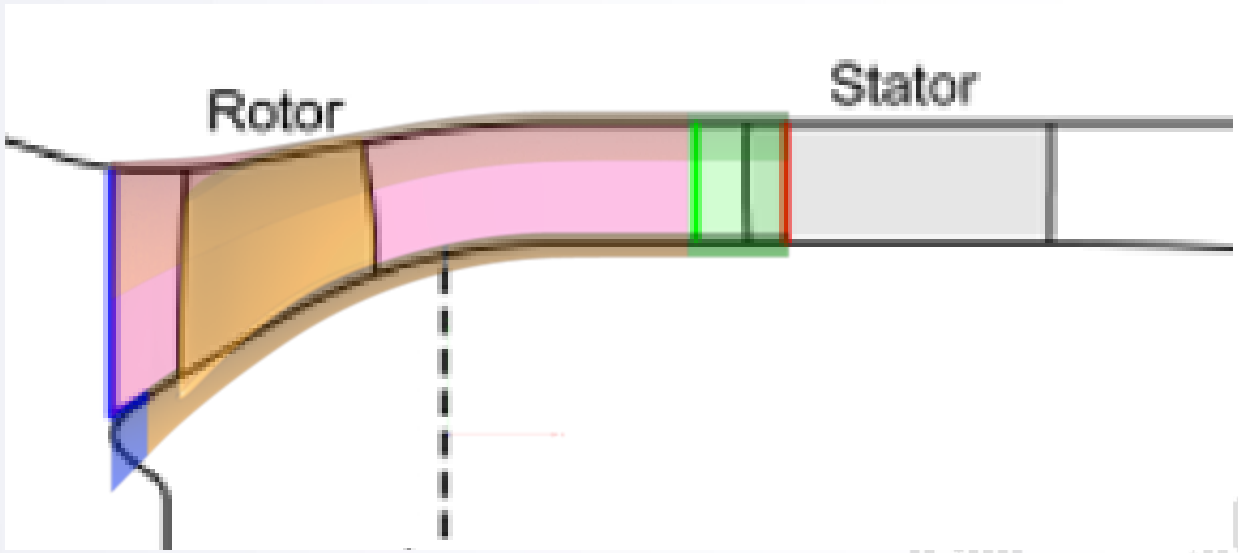

Meridional View

Results

Spacecraft Cabin Ventilation Fan

Computational Grid

- 2,323,333 Cells

Tet	Pyr	Pri	Hex
820K	56K	1.1M	336K

- Degrees of Freedom

P1	P2	P3	P4
13M	38M	84M	157M

Computational Setup

- Implicit LES (no subgrid modeling)
- 11-stage/3rd-order vortex-optimized Runge-Kutta

Boundary Conditions

- Hub, rotor, and case walls set to no-slip adiabatic
  - Hub and rotor in MRF → zero wall velocity
  - Case in inertial reference frame → -Ω rotational speed imposed at the wall
- Subsonic inflow specifying total conditions
  - Inflow only in axial direcition
  - No inflow turbulence
- Subsonic outflow setting a static pressure ratio relative to the inflow conditions
- Rotationally periodic

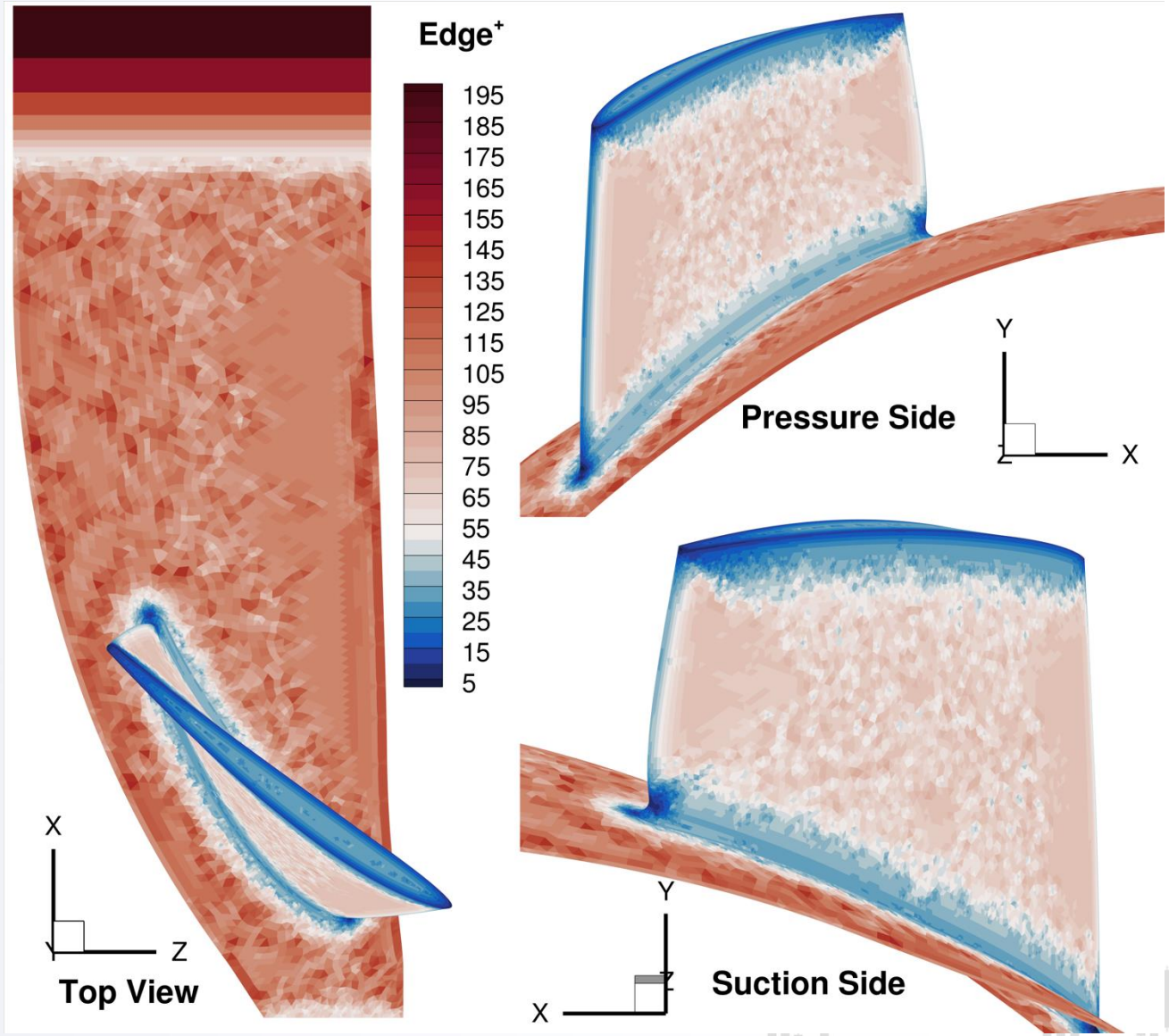

Edge length of surface mesh elements in wall units.

Results

Spacecraft Cabin Ventilation Fan

Fan performance map using P1 simulations

- 16 total P1 operating points using PR = 1.0025–1.0078
- The experimental data is included to gauge if the GFR results are reasonable.
  - Experiment contains rotor+stator so not a one-to-one comparison.
- Notable operating points:
  - PR=1.0055
    - Peak efficiency at 144 CFM
  - PR=1.0077
    - Peak ΔP_0 at 110 CFM
  - PR=1.00775 and PR=1.0078
    - Plummeting CFM indicates stall
- Peak efficiency also run at P3.
  - Lower dissipation results in slightly higher CFM, ΔP_0, and adiabatic efficiency than P1.

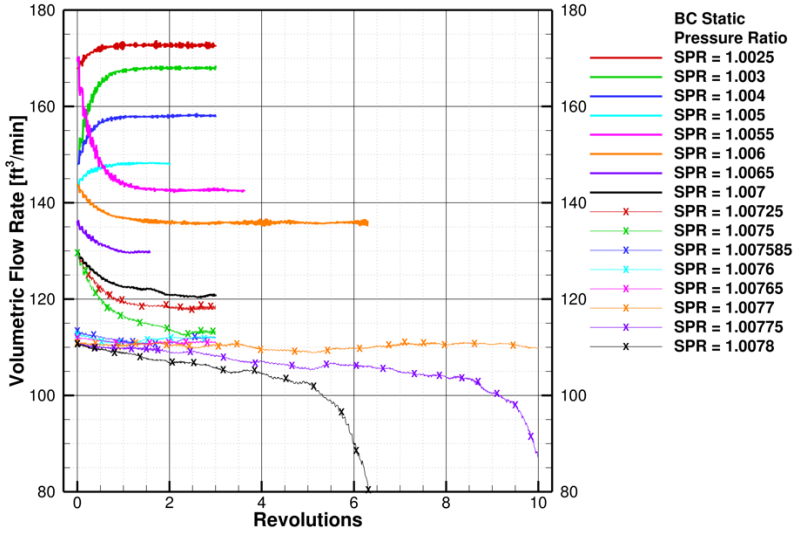

Convergence of CFM for P1 cases

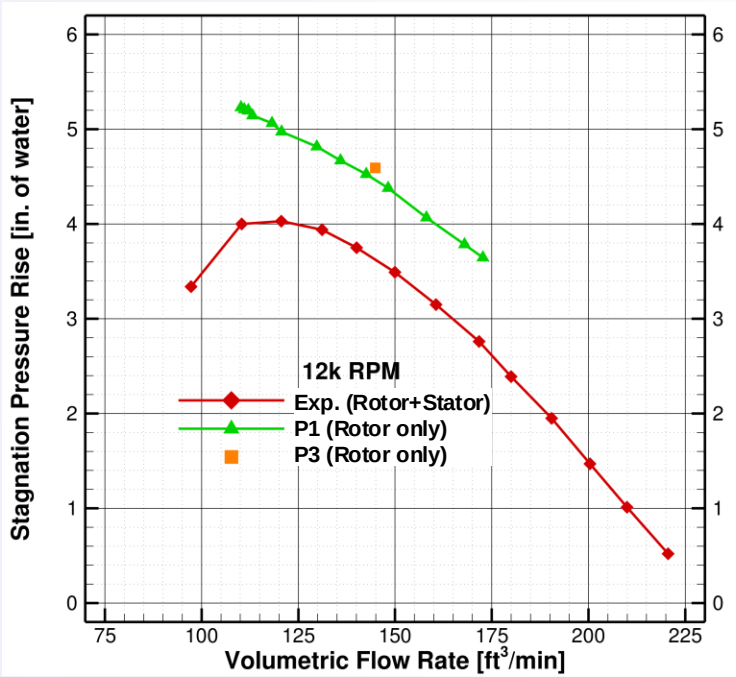

CFM vs. ΔP_0

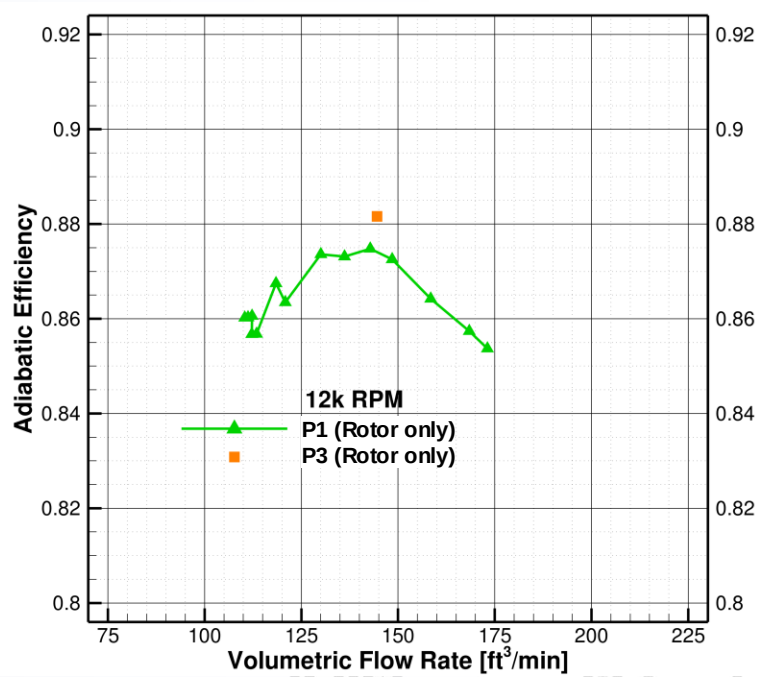

CFM vs. Adiabatic Efficiency

Results

Spacecraft Cabin Ventilation Fan

Fan performance map using P1 simulations

- 16 total P1 operating points using PR = 1.0025–1.0078
- The experimental data is included to gauge if the GFR results are reasonable.
  - Experiment contains rotor+stator so not a one-to-one comparison.
- Notable operating points:
  - PR=1.0055
    - Peak efficiency at 144 CFM
  - PR=1.0077
    - Peak ΔP_0 at 110 CFM
  - PR=1.00775 and PR=1.0078
    - Plummeting CFM indicates stall
- Peak efficiency also run at P3.
  - Lower dissipation results in slightly higher CFM, ΔP_0, and adiabatic efficiency than P1.

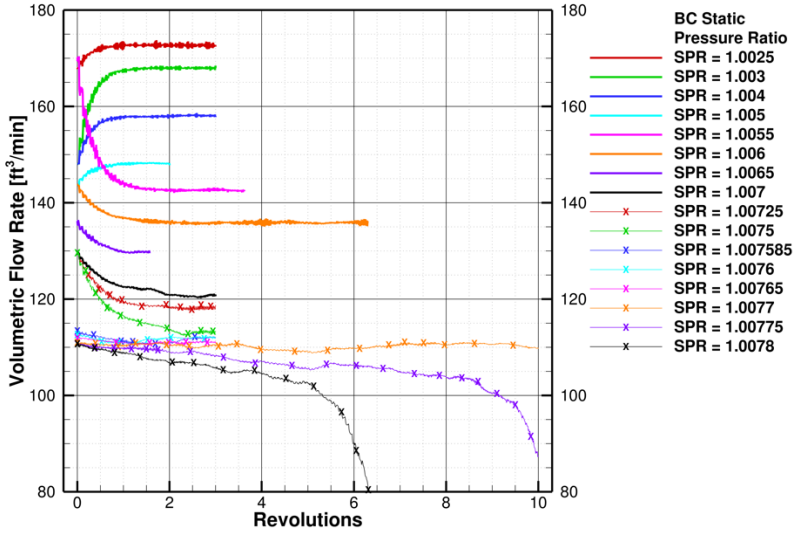

Convergence of CFM for P1 cases

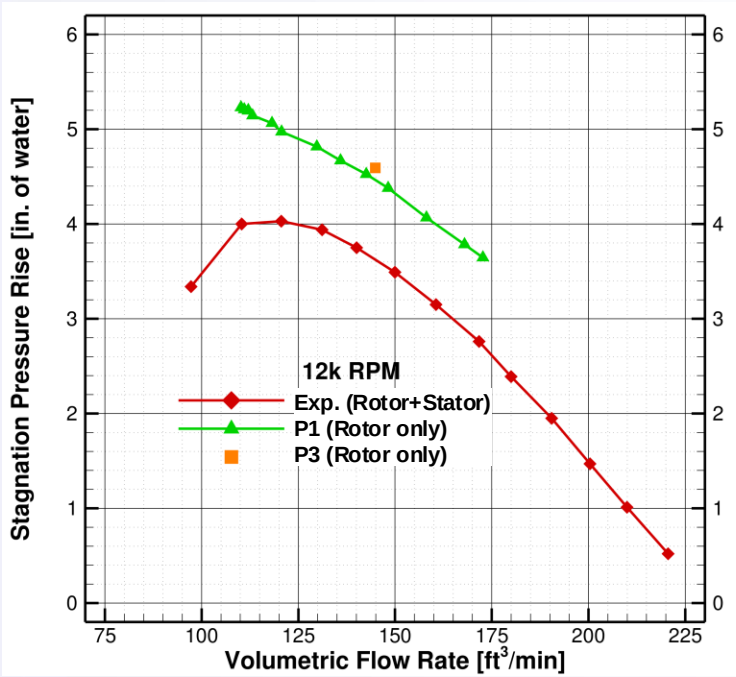

CFM vs. ΔP_0

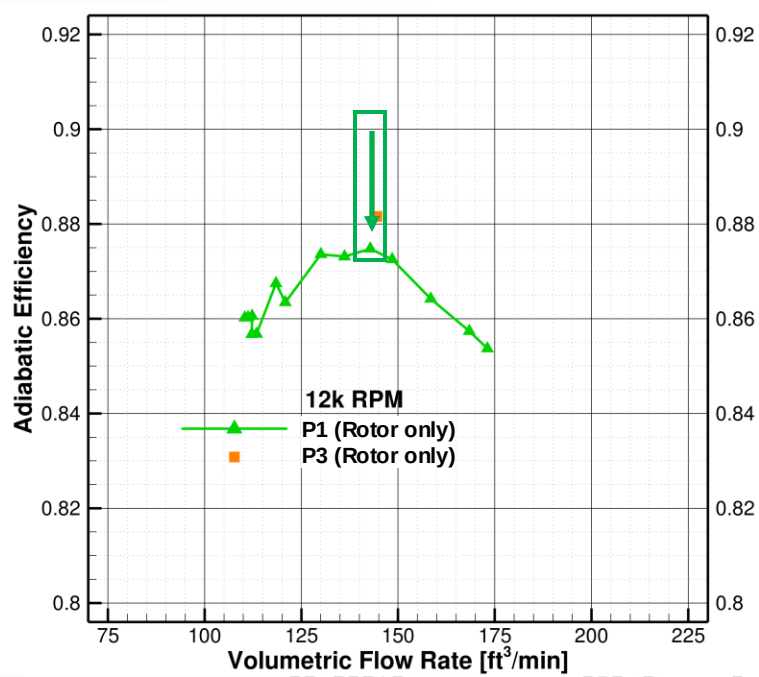

CFM vs. Adiabatic Efficiency

Results

Spacecraft Cabin Ventilation Fan

Fan performance map using P1 simulations

- 16 total P1 operating points using PR = 1.0025–1.0078
- The experimental data is included to gauge if the GFR results are reasonable.
  - Experiment contains rotor+stator so not a one-to-one comparison.
- Notable operating points:
  - PR=1.0055
    - Peak efficiency at 144 CFM
  - PR=1.0077
    - Peak ΔP_0 at 110 CFM
  - PR=1.00775 and PR=1.0078
    - Plummeting CFM indicates stall
- Peak efficiency also run at P3.
  - Lower dissipation results in slightly higher CFM, ΔP_0, and adiabatic efficiency than P1.

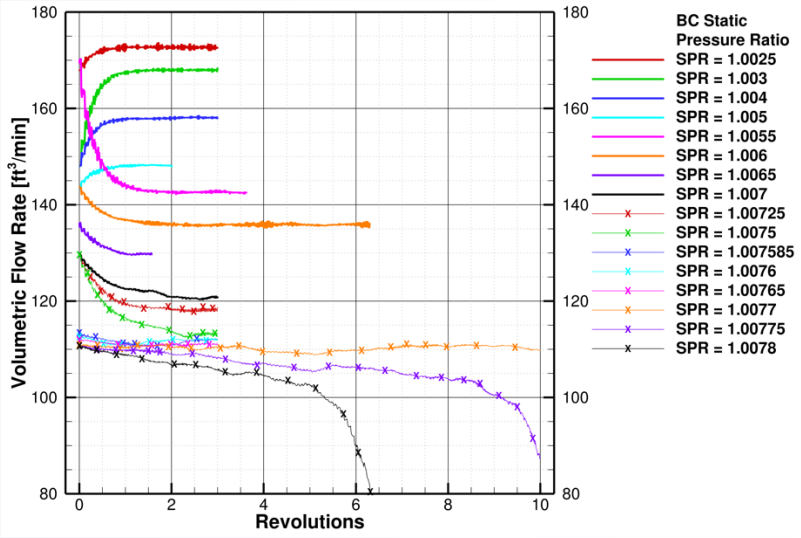

Convergence of CFM for P1 cases

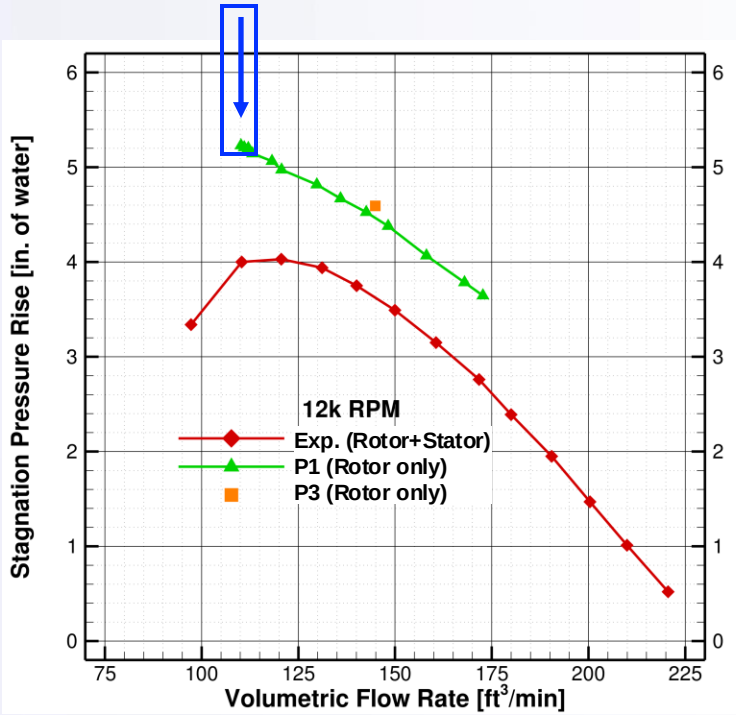

CFM vs. ΔP_0

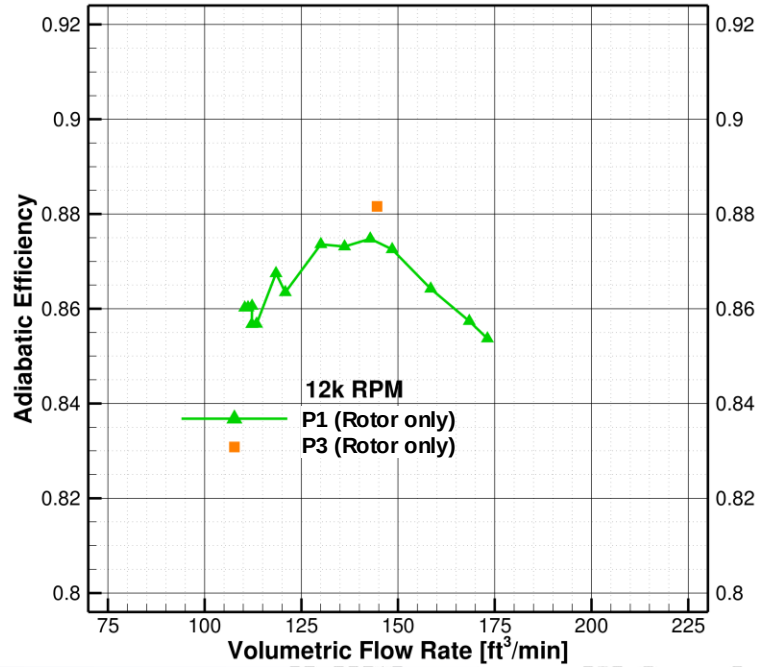

CFM vs. Adiabatic Efficiency

Results

Spacecraft Cabin Ventilation Fan

Fan performance map using P1 simulations

- 16 total P1 operating points using PR = 1.0025–1.0078
- The experimental data is included to gauge if the GFR results are reasonable.
  - Experiment contains rotor+stator so not a one-to-one comparison.
- Notable operating points:
  - PR=1.0055
    - Peak efficiency at 144 CFM
  - PR=1.0077
    - Peak ΔP_0 at 110 CFM
  - PR=1.00775 and PR=1.0078
    - Plummeting CFM indicates stall
- Peak efficiency also run at P3.
  - Lower dissipation results in slightly higher CFM, ΔP_0, and adiabatic efficiency than P1.

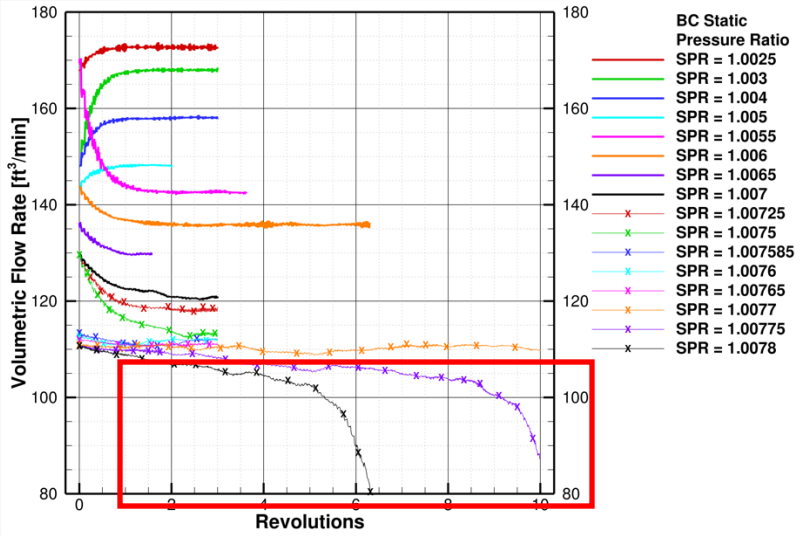

Convergence of CFM for P1 cases

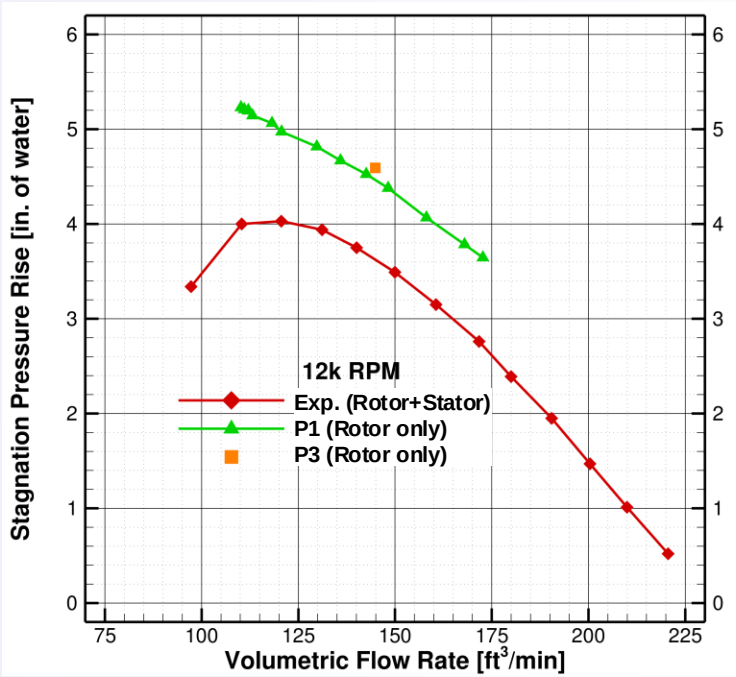

CFM vs. ΔP_0

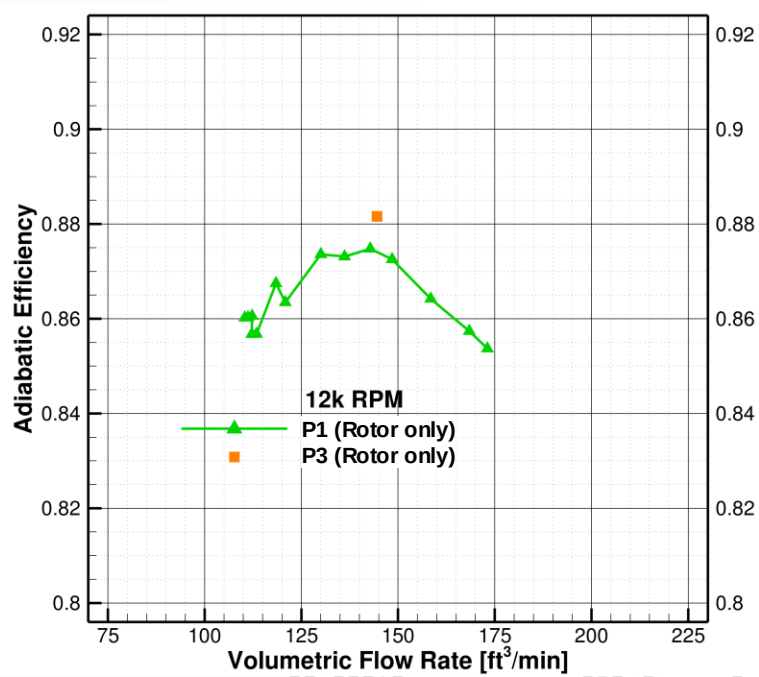

CFM vs. Adiabatic Efficiency

Results

Spacecraft Cabin Ventilation Fan

Fan performance map using P1 simulations

- 16 total P1 operating points using PR = 1.0025–1.0078
- The experimental data is included to gauge if the GFR results are reasonable.
  - Experiment contains rotor+stator so not a one-to-one comparison.
- Notable operating points:
  - PR=1.0055
    - Peak efficiency at 144 CFM
  - PR=1.0077
    - Peak ΔP_0 at 110 CFM
  - PR=1.00775 and PR=1.0078
    - Plummeting CFM indicates stall
- Peak efficiency also run at P3.
  - Lower dissipation results in slightly higher CFM, ΔP_0, and adiabatic efficiency than P1.

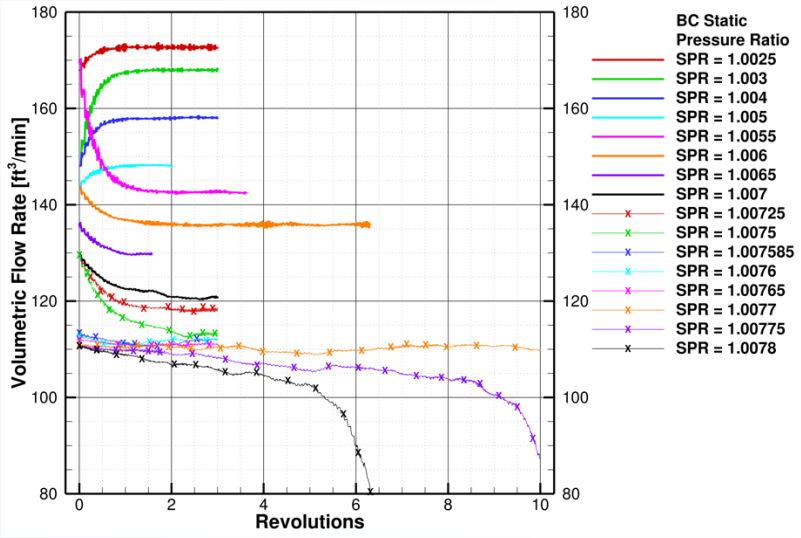

Convergence of CFM for P1 cases

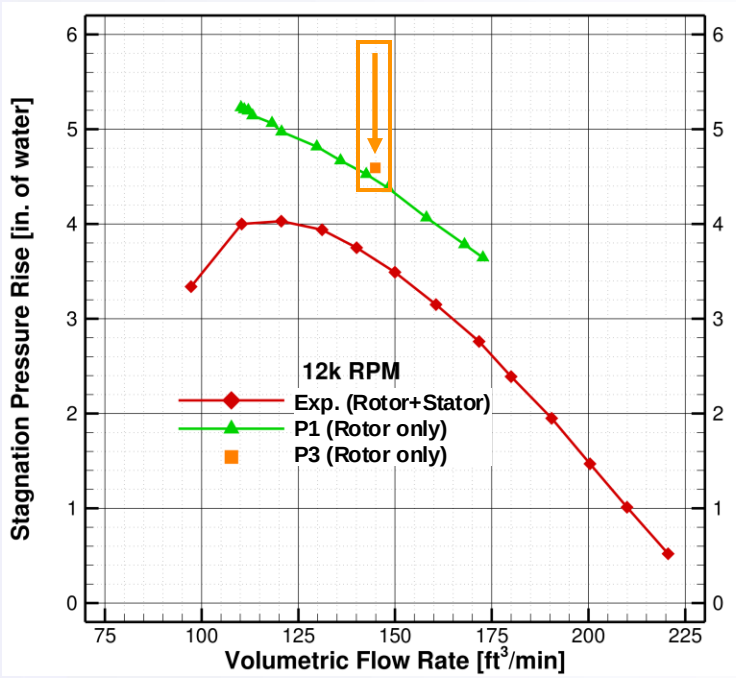

CFM vs. ΔP_0

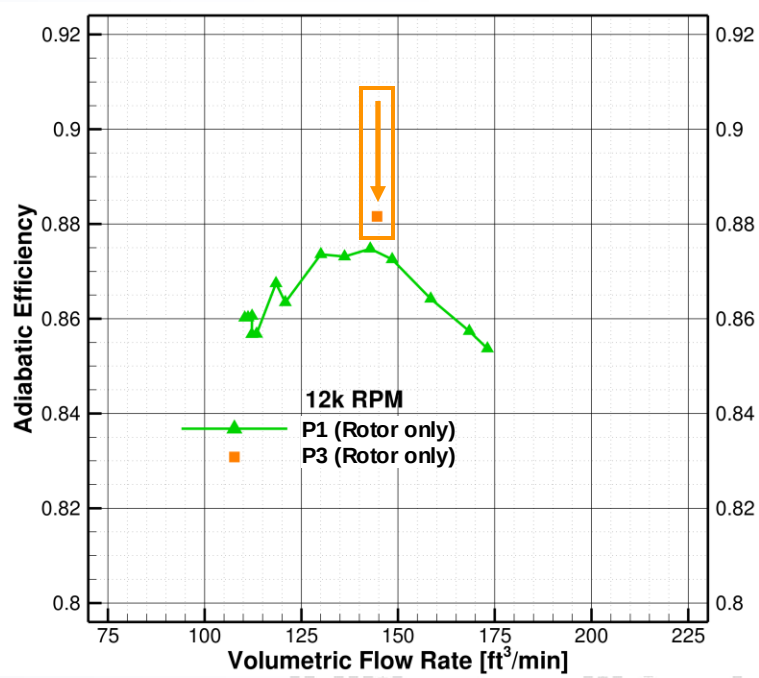

CFM vs. Adiabatic Efficiency

Results

Spacecraft Cabin Ventilation Fan

Flow details vs. P order

- Starting with same P1 solution, P1-P4 simulations were run for 0.2522 revolutions.
- Slices taken at 99% passage height.
  - We are looking at the flow over the blade tips, which are located just underneath the screen.
  - Located within the tip gap, just above the blade.
- P1 resolves all the major flow features.
  - Misses the T-S waves above the tip.
  - No structures within the leading edge wake.

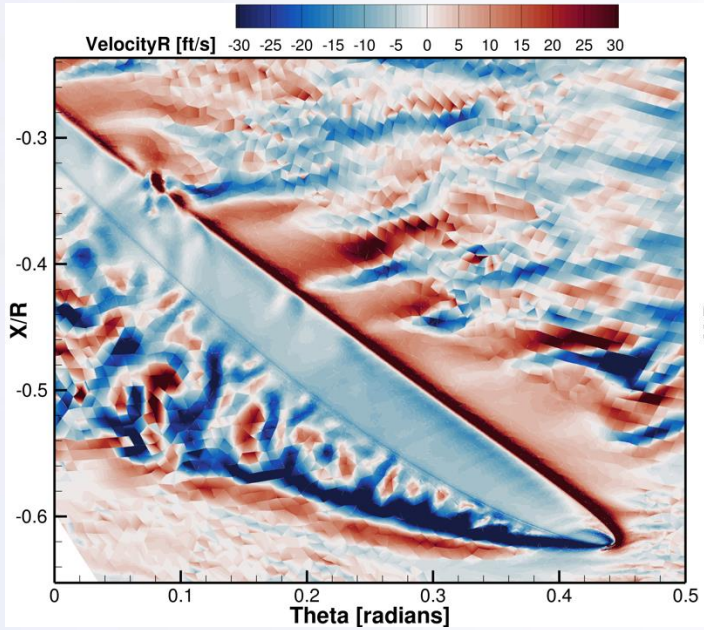

P1 with 13 million DoF

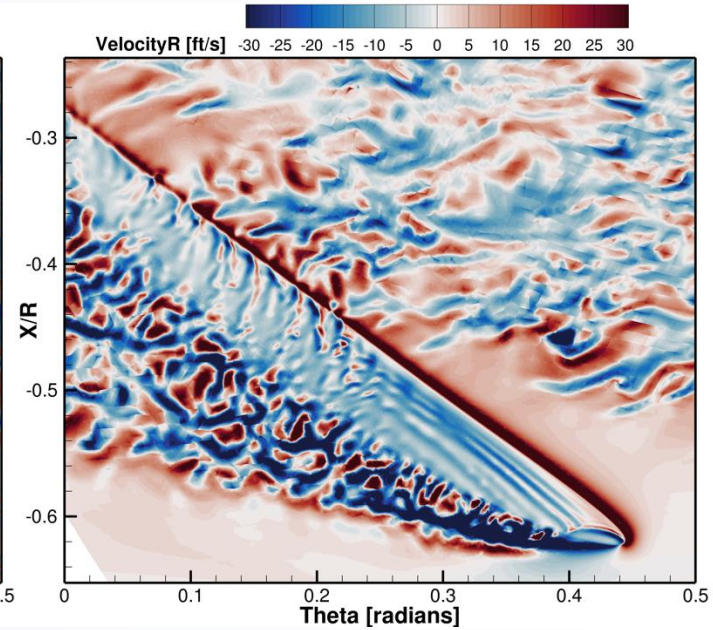

P2 with 38 million DoF

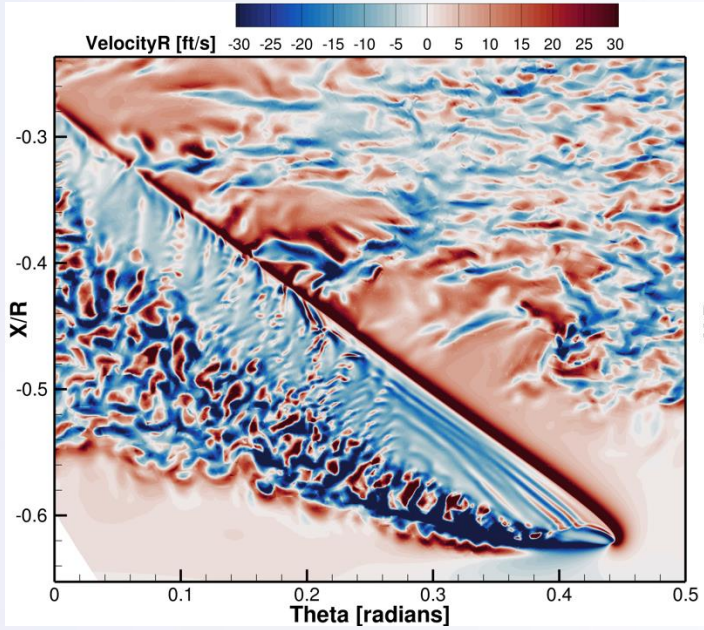

P3 with 84 million DoF

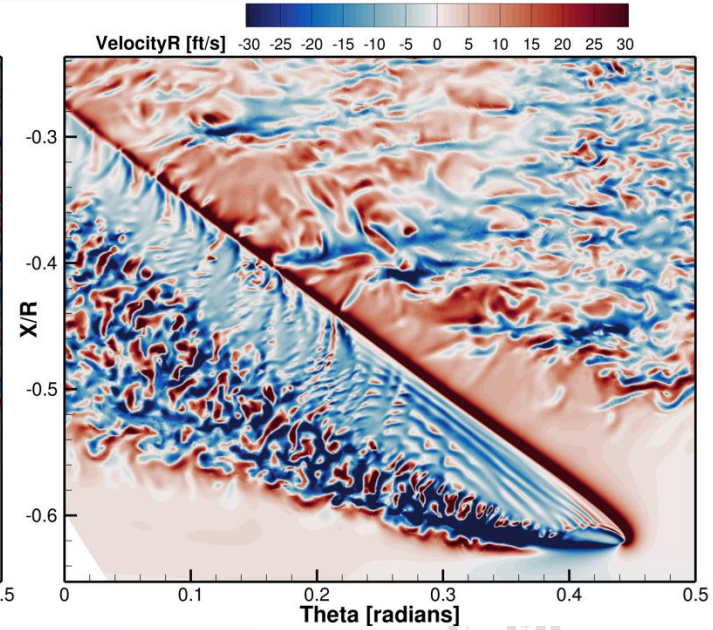

P4 with 157 million DoF

Results

Spacecraft Cabin Ventilation Fan

P4 animation at PR = 1.0077 (peak ΔP0)

- Slice taken at 99% passage height.
- Looking at the flow over the blade tips, which are located just underneath the screen.
- Flow is moving bottom to top.
- Post-processing tools were used to create this multi-blade flow by replicating the single blade solution.

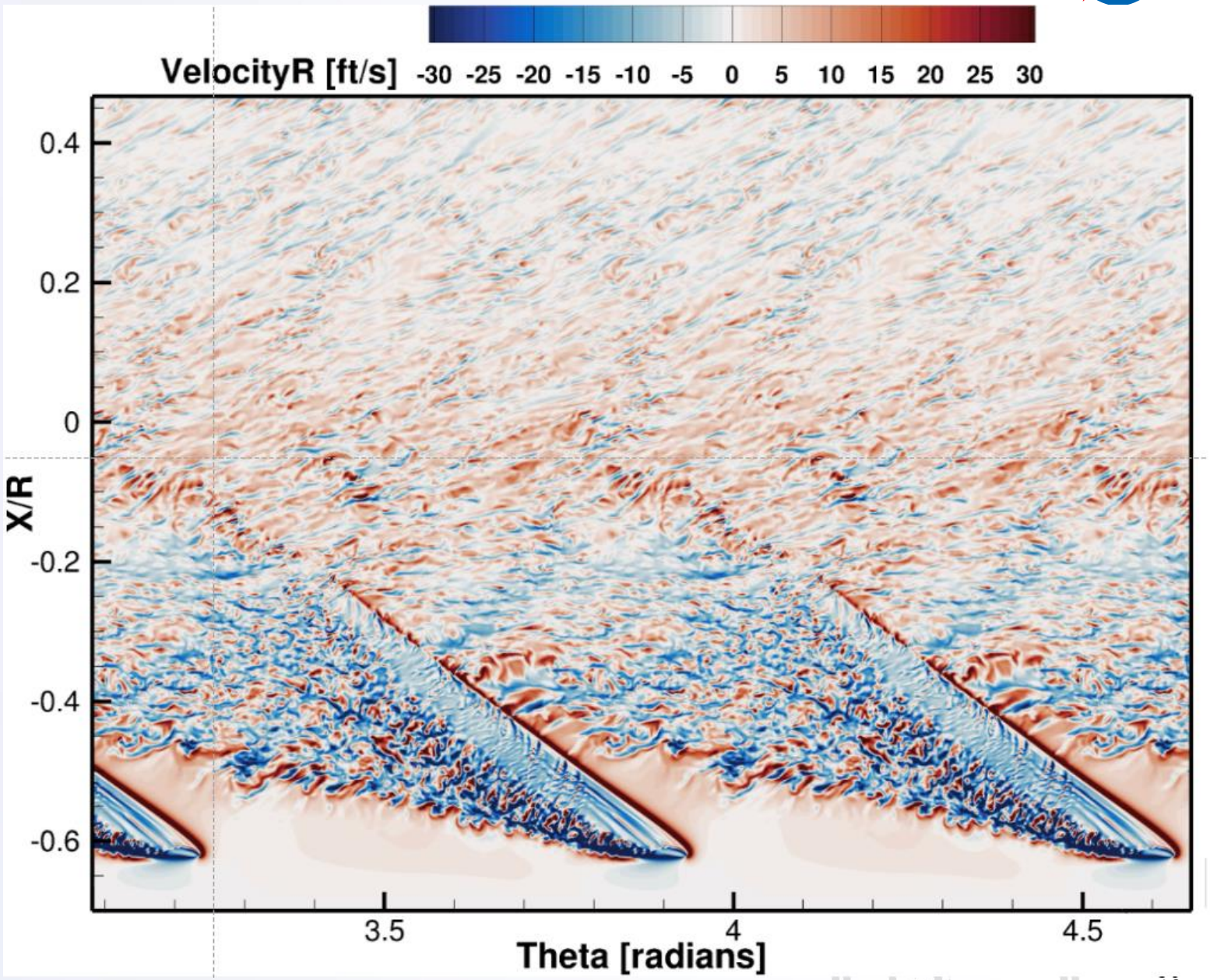

Results

Spacecraft Cabin Ventilation Fan

P4 streamtraces at PR = 1.0055 (peak efficiency)

- Further verification against currently limited and future experimental measurements still needed.
- Potential for new insights into the fluid dynamics for this and similar configurations not found/detectable by RANS or experiment.

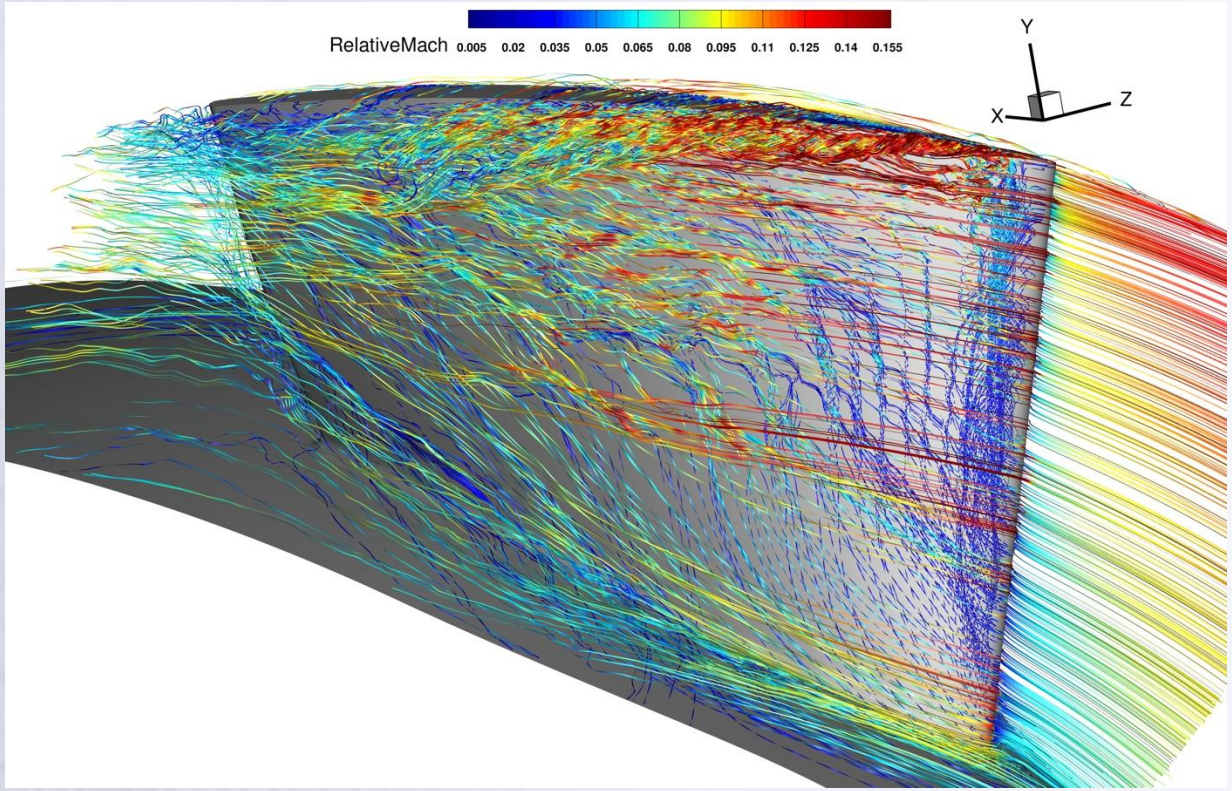

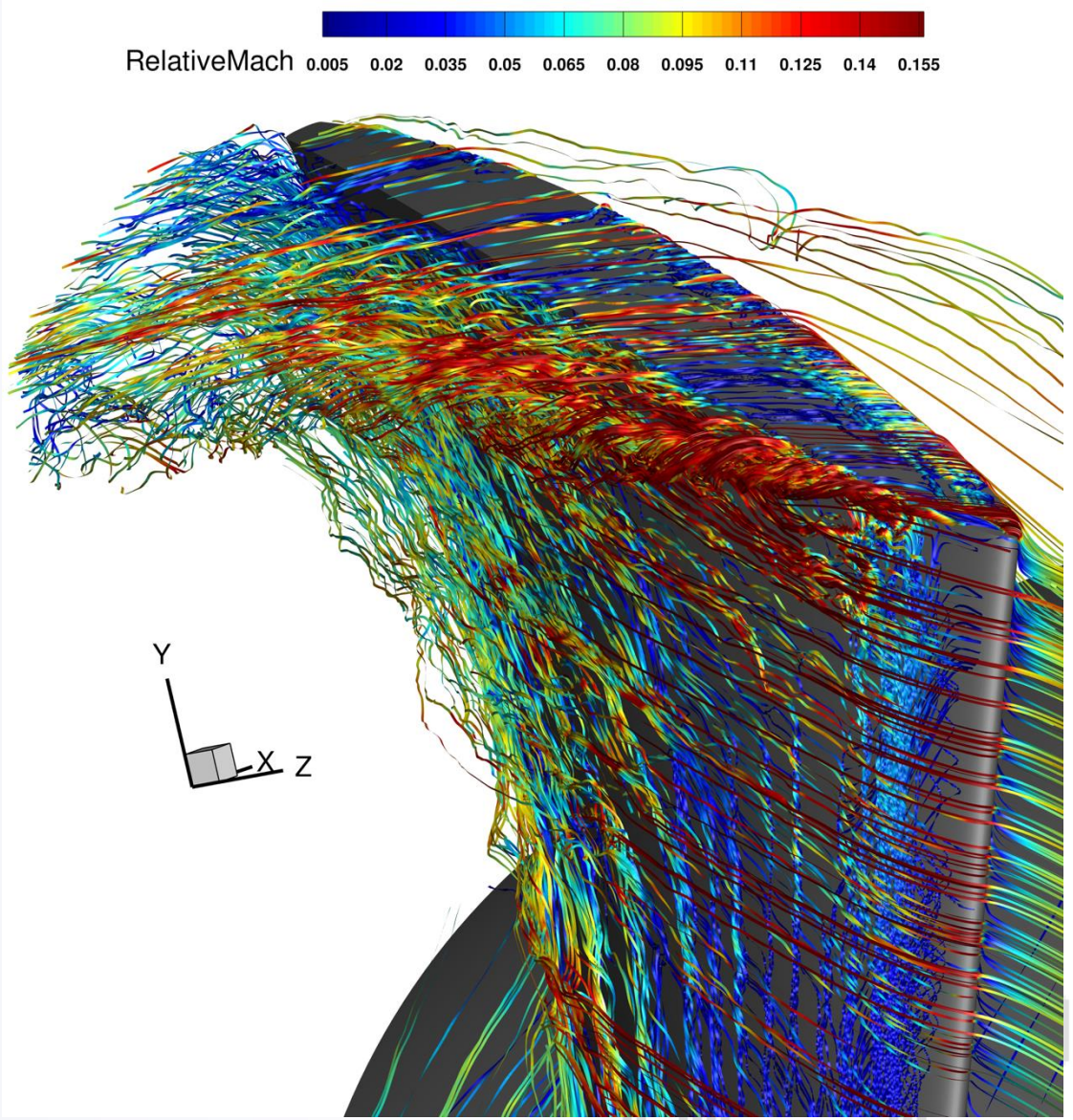

Results

Spacecraft Cabin Ventilation Fan

P4 streamtraces at PR = 1.0055 (peak efficiency)

- Further verification against currently limited and future experimental measurements still needed.

Significance:

- First successful simulations demonstrating the new rotating turbomachinery capability in GFR.
- Demonstration of the new mixed-element mesh capability towards real-world problem.
- High-order solutions show potential for new insights into the fluid dynamics for this and similar configurations not found/detectable by RANS or experiment.

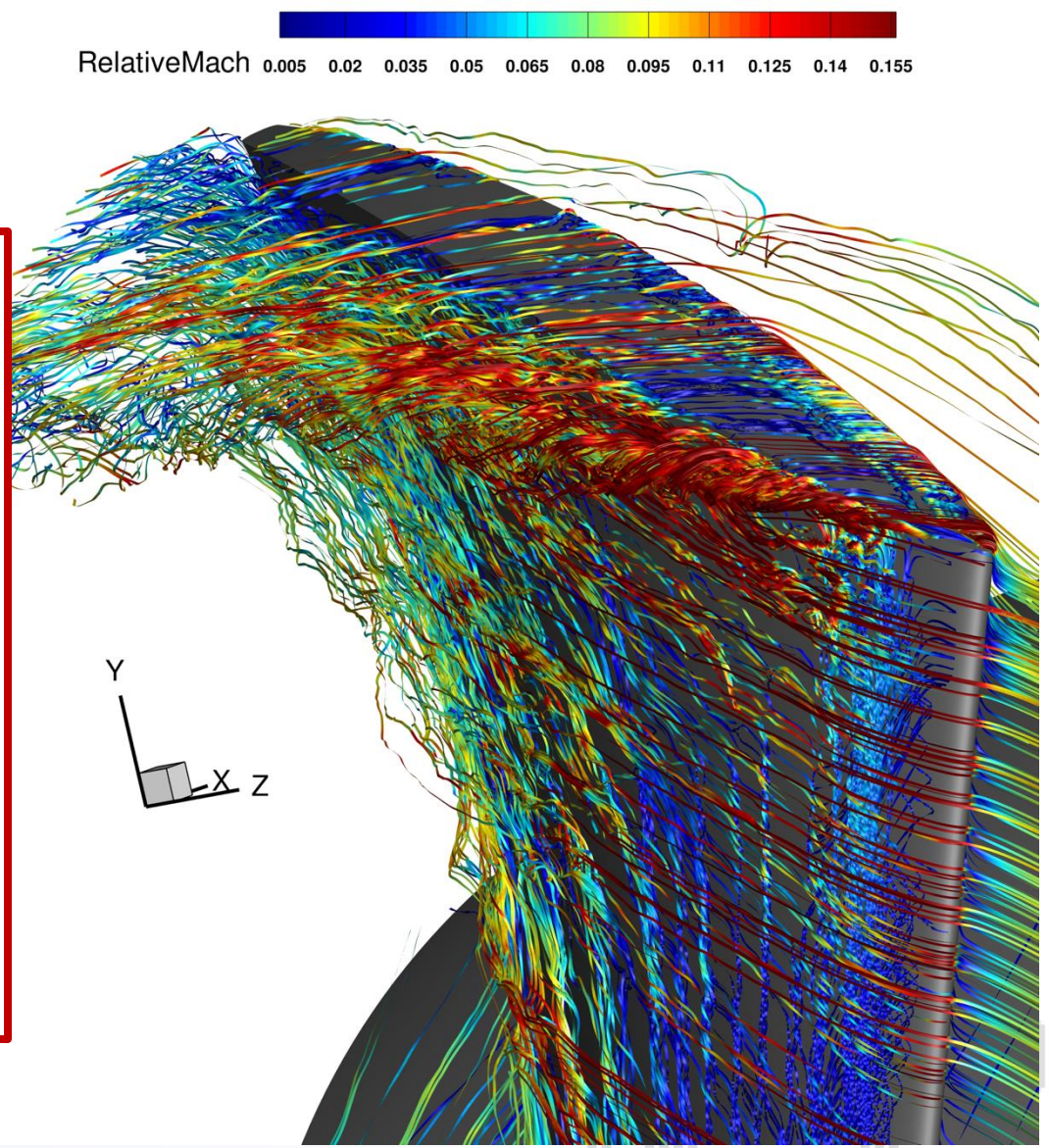

Summary

New Capabilities and Improvements

- Added several explicit RK methods demonstrating 20-30% time-to-solution improvements.
- Added and verified 3D mixed element and rotating reference frame capabilities.

Applications

- Paper: Demonstrated unstructured mixed-element mesh capability using Taylor-Green vortex.
- Paper: Used Turbulent Heat Flux – Phase 3 (single-hole cooling flow) for verification and validation of LES capability for flows with complex aerodynamic and thermodynamic interactions.
- The spacecraft cabin ventilation fan was used to demonstrate that GFR is ready for rotating turbomachinery applications where high-order LES is preferable to RANS approaches.
  - Used P1 to efficiently establish a full fan performance map.
  - Demonstrated the potential use of higher-order “deep dives” on selective operating points for further insights and analysis of the fluid dynamics.

Future Work

- Support for running on GPUs.
- Sliding mesh interface capability for coupled rotor/stator simulations.
- Add wall-modeled LES capability to reduce grid resolution required for LES of wall-bounded flows.
- Improved shock-capturing with minimal tuning for flows involving shocks.

Acknowledgements

This research was sponsored by NASA's Transformational Tools and Technologies (TTT) Project of the Transformative Aeronautics Concepts Program under the Aeronautics Research Mission Directorate.

Computing resources were provided by the NASA High-End Computing (HEC) Program through the NASA Advanced Supercomputing (NAS) Division at Ames Research Center.

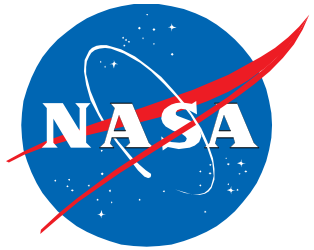
NASA